Polymer 49 (2008) 2845–2856

Contents lists available at ScienceDirect

Polymer

journal homepage: www.elsevier.com/locate/polymer

Synthesis and characterization of liquid crystalline copolymers with dual photochromic pendant groups

Po-Chih Yang, Ming-Zu Wu, Jui-Hsiang Liu*

Department of Chemical Engineering, National Cheng Kung University, No. 1, University Road, Tainan 70101, Taiwan, ROC

ARTICLE INFO

Article history:
Received 5 March 2008
Received in revised form 13 April 2008
Accepted 17 April 2008
Available online 25 April 2008

Keywords:
Chiral
Photochemistry
Isomerization

ABSTRACT

In order to study the photoreactivity and the optical properties of liquid crystalline copolymers with multiple photochromic groups, a series of novel liquid crystalline binary and ternary polyacrylates consisting of one (C═C or N═N) or dual (C═C and N═N) photochromic segments were synthesized and characterized considering their liquid crystalline, optical, and photochromic properties and their thermal stability. Achiral homopolymer **P1** shows a smectic A phase (fan-shaped texture), and all chiral copolymers **CP1**–**CP6** exhibit chiral nematic phases (cholesteric, oily streaks textures). The polymers show excellent solubility in common organic solvents such as chloroform, toluene, and THF. These polymers also exhibit good thermal stability, with decomposition temperatures (T_ds) greater than 373 °C at 5% weight loss, and beyond 440 °C at 50% weight loss under nitrogen atmosphere. UV irradiation caused *E*/*Z* photoisomerization at N═N and C═C segments of the synthesized photochromic copolymers leading to reversible and irreversible isomerizations, respectively. The synthesized liquid crystalline ternary copolymer **CP6**, containing two different photochromic N═N and C═C groups, is sensitive to different UV wavelengths and is notably interesting from the viewpoint of photochromic copolymers.

1. Introduction

Liquid crystalline polymers (LCPs) containing photochromic groups have promising practical applications, such as reversible optical data recording, and use in the preparation of command surfaces and holography [1–5]. Highly promising candidates are cholesteric polymers and their compositions with low molecular weight liquid crystals, with unique helical supramolecular structures. This supramolecular structure may be easily controlled by light irradiation. This trend opens the possibilities for the preparation of so-called photorecorded films with locally variable supramolecular structures and optical properties [6–11]. An interesting and novel method for reversibly modifying the optical properties of polymers is photoinduced variation of the degree of ordering, alignment direction, and its distribution or the morphology of polymers by various processes. Photoinduced modification of ordering in polymers has been used for information storage [12–15].

The development of photosensitive media based on liquid crystalline compounds for data recording, optical storage, and reproduction is one of the most rapidly developing areas in the physical chemistry of low molecular mass and polymer liquid crystals. Photocontrolled cholesteric polymers introduce photosensitive or photoisomerized mesogenic fragments such as azobenzene [11,16] and stilbene [4,17], which can reverse their configurations when irradiated with different light wavelengths. Any change in the configuration of the polymer changes the twisting power and optical characteristics simultaneously. This approach has allowed the preparation of photo-addressable materials, whose helical pitch may be easily controlled by light irradiation, via changes in the twisting power of chiral photochromic fragments associated with changes in their configuration. Combined LC copolymers containing both azobenzene and chiral photochromic groups also have generated great interest.

In a series of studies, chiral monomers and chiral dopants were synthesized, and their applications in the induction of cholesteric liquid crystal phases were studied [18–22]. In these studies, the photochromic function was designed with azobenzene derivatives. To overcome the thermal stability of the photochromic pendant group, photochromic compounds with C═C segments were synthesized, and their optical properties and thermal stabilities were also characterized [23]. In this investigation, to study the photoreactivity of liquid crystalline copolymers with multiple photochromic groups, a series of binary and ternary liquid crystalline copolymers were synthesized, and their physical properties were also well characterized. The photochromic properties and thermal stability of these polymers are presented in detail. The results of this investigation present significant scientific and practical

* Corresponding author. Tel.: +886 6 2757575x62646; fax: +886 6 2384590.
E-mail address: jhliu@mail.ncku.edu.tw (J.-H. Liu).

0032-3861/$ – see front matter © 2008 Elsevier Ltd. All rights reserved.
doi:10.1016/j.polymer.2008.04.036

contributions with respect to the development of unique multifunctional photochromic polymer materials.

2. Experimental

2.1. Materials

4-Hydroxybenzoic acid (99.0%), 6-chloro-1-hexanol (95.0%), acryloyl chloride (98.0%), L(−)-menthol (99.7%; $[\alpha]_D = -51°$, $c = 10$ in EtOH), (*S*)-(−)-2-methyl-1-butanol (99.0%; $[\alpha]_D = -5.8°$), 4-hexyloxyphenol (99.0%), *N*,*N*′-dicyclohexylcarbodiimide (DCC; 99.0%), and 2,2′-azobisisobutyronitrile (AIBN; 98.0%) were purchased from Acros Chemical Co. 4-Dimethylaminopyridine (DMAP; 99.0%) was purchased from Lancaster Chemical Co. 4-(6-Acryloyloxyhexyloxy) benzoic acid, 4-(6-acryloyloxyhexyloxy) cinnamic acid, (*S*)-(−)-2-methyl-butyl 4-hydroxybenzoate, (−)-menthyl 4-hydroxybenzoate, and 4-hexyloxyphenyl-4′-(6-acryloyloxyhexyloxy) benzoate (**M1**) were synthesized by following the procedures described in the literature [22,24]. All organic solvents were purchased from Aldrich Chemical Co. Dichloromethane (CH_2Cl_2) was distilled over calcium hydride under argon immediately before use, and other solvents were purified by standard methods. Analytical thin-layer chromatography was conducted on Merck aluminum plates with 0.2 mm of silica gel 60F-254. Anhydrous sodium sulfate was used to dry all organic extracts. AIBN was freshly recrystallized from methanol.

2.2. Measurements

FTIR spectra were recorded as a KBr disk on a Jasco VALOR III (Tokyo, Japan) FTIR spectrophotometer. ^{1}H and ^{13}C NMR spectra were obtained on a Bruker AMX-400 (Darmstadt, Germany) high-resolution NMR spectrometer, and chemical shifts were reported in ppm with tetramethylsilane (TMS) as an internal standard. Optical rotations were measured at 30 °C in chloroform using a Jasco DIP-370 polarimeter with the D-line of sodium ($\lambda = 589$ nm) with a precision of ±0.001°. The measurements were performed using 1% solutions of the substances in chloroform. Elemental analyses were carried out on a Heraeus CHN-O (Darmstadt, Germany) rapid elemental analyzer. Gel permeation chromatographic (GPC) measurements were carried out at 40 °C on a Hitachi L-4200 (Osaka, Japan) instrument equipped with a TSK gel GMH and G2000H columns using $CHCl_3$ as an eluent. The rate of elution was 1.0 mL min^{-1}, and the instrument was calibrated with a polystyrene standard. Differential scanning calorimetry (DSC) was conducted with a Perkin Elmer DSC 7 at a heating and a cooling rate of 10 K min^{-1} under nitrogen atmosphere. The phase transitions were investigated by an Olympus BH-2 polarized light microscope (POM) equipped with a Mettler hot stage FP-82. The temperature scanning rates were determined at a rate of 10 K min^{-1}. Thermal decomposition temperature data were recorded under nitrogen atmosphere at a heating rate of 40 K min^{-1} with a thermogravimetric analyzer (TGA) Perkin Elmer TGA 7. UV–vis absorption spectra were measured with a Jasco V-550 spectrophotometer. The X-ray diffraction data were recorded on a Rigaku RINT 2500 series instrument with Ni-filtered Cu Kα radiation. The sample in a quartz capillary was held in a temperature-controlled cell (Rigaku LC high-temperature controller). Scanning electron microscopic (SEM) microphotographs were measured with a JEOL HR-FESEM JSM-6700F (Osaka, Japan) instrument. UV light (300 nm; Model UVG-54) with an intensity of 0.6 mW was used as the pumping light to induce photoisomerization of chiral monomers with C=C bonds in chloroform solutions. UV light (365 nm; Model UVG-56) with an intensity of 0.4 mW was used as the pumping light to induce photoisomerization of azo compounds with N=N bonds in $CHCl_3$ solutions. Nominal resolution mass spectra were recorded using an analytical mass spectrometer (Fast Atom Bombardment Mass Spectroscopy, FABMS), model JEOL JMS-700.

2.3. Synthesis of monomers (Scheme 2)

Compounds **M1**–**M5** were synthesized according to the literature [25–29] and our previous reports [19,22–24]. The obtained products were purified and then identified using ^{1}H, ^{13}C NMR, and FTIR spectra, as well as elemental analysis.

2.3.1. (*S*)-(+)-2-Methyl-butyl 4-(6-acryloyloxyhexyloxy) phenyl-4′-benzoate (***M2***)

4-(6-Acryloyloxyhexyloxy) benzoic acid (2.92 g, 10.0 mmol) and (*S*)-(−)-2-methyl-butyl 4-hydroxybenzoate (2.50 g, 12.0 mmol) were dissolved in dry CH_2Cl_2 (50 mL) at 30 °C. *N*,*N*′-Dicyclohexylcarbodiimide (DCC; 3.09 g, 15.0 mmol) and 4-dimethylaminopyridine (DMAP; 0.12 g, 1 mmol) were dissolved in CH_2Cl_2 (30 mL), and then added to the solution. The reaction mixture was stirred for 24 h at 30 °C. A solid, *N*,*N*′-dicyclohexyl urea, was precipitated and filtered off. The resulting solution was filtered and washed with water, dried with anhydrous $MgSO_4$, and evaporated to dryness. The crude product was purified by column chromatography (silica gel, ethyl acetate/hexane = 1/5). Yield: 2.44 g (50.6%). K 16.8 °C S_A^* 24.0 °C I. $[\alpha]_D = +3.2°$. FTIR (KBr pellet, ν_{max}/cm^{-1}): 2930, 2872 (CH_2), 1710 (C=O in Ar–COO–), 1606, 1512 (C–C in Ar), 1198, 1228 (COC), 1678 (C=C). ^{1}H NMR ($CDCl_3$, δ in ppm): 0.93–1.02 (m, 6H, CH_3), 1.26–1.88 (m, 11H, CH_2), 4.03–4.06 (t, 2H, CH_2OPh, J = 6.43 Hz), 4.11–4.23 (m, 4H, $COOCH_2$, J = 6.65 Hz), 5.80–5.83 (dd, 1H, CH_2=CH, J = 10.37 Hz), 6.08–6.15 (dd, 1H, CH_2=CH, J_1 = 10.38 Hz, J_2 = 6.95 Hz), 6.38–6.42 (dd, 1H, CH_2=CH, J = 17.28 Hz), 6.95–7.00 (d, 2H, Ar–H, J = 8.48 Hz), 7.26–7.31 (d, 2H, Ar–H, J = 8.51 Hz), 8.07–8.16 (d, 4H, Ar–H, J = 8.35 Hz). ^{13}C NMR (100.6 MHz, $CDCl_3$): 15.44 (CH_3), 24.81, 25.68, 26.31, 28.75, 29.22, 34.56 (CH_2), 62.99, 68.16, 69.18 (OCH_2), 113.16, 121.35, 128.80, 129.51 (aromatic), 128.80, 131.86 (C=C), 120.56, 125.20, 152.26, 159.72 (aromatic quaternary), 165.88, 166.31, 167.07 (C=O). Anal calcd for $C_{28}H_{34}O_7$: C 69.70, H 7.05; found: C 69.82, H 7.01%. FABMS (m/z) 482 M^+.

2.3.2. (−)-Menthyl 4-(6-acryloyloxyhexyloxy) phenyl-4′-benzoate (***M3***)

Yield: 42.0%. T_m = 32.6 °C. $[\alpha]_D = -46.2°$. FTIR (KBr pellet, ν_{max}/cm^{-1}): 2934, 2870 (CH_2), 1712 (C=O in Ar–COO–), 1610, 1505 (C–C in Ar), 1196, 1230 (COC), 1682 (C=C). ^{1}H NMR ($CDCl_3$, δ in ppm): 0.77–0.94 (m, 9H, CH_3), 1.09–2.11 (m, 17H, CH_2), 4.00–4.07 (t, 2H, CH_2OPh, J = 6.33 Hz), 4.16–4.20 (t, 2H, $COOCH_2$, J = 6.59 Hz), 4.90–4.97 (m, 1H, $OCHCH_2$), 5.80–5.83 (dd, 1H, CH_2=CH, J = 10.33 Hz), 6.09–6.16 (dd, 1H, CH_2=CH, J_1 = 10.41 Hz, J_2 = 6.92 Hz), 6.38–6.42 (dd, 1H, CH_2=CH, J = 17.38 Hz), 6.96–6.99 (d, 2H, Ar–H, J = 8.58 Hz), 7.26–7.29 (d, 2H, Ar–H, J = 8.19 Hz), 8.10–8.16 (d, 4H, Ar–H, J = 8.3 Hz). ^{13}C NMR (100.6 MHz, $CDCl_3$): 21.06, 22.03 (CH_3), 23.17, 25.70, 28.77, 34.22, 39.05, 62.99, 68.16 (CH_2), 62.99, 68.17 (OCH_2), 24.68, 29.70, 48.31, 75.44 (CH), 113.15, 121.23, 128.15, 129.52 (aromatic), 128.80, 131.85 (C=C), 120.56, 125.17, 152.26, 159.71 (aromatic quaternary), 165.88, 166.30, 167.31 (C=O). Anal calcd for $C_{33}H_{42}O_7$: C 72.00, H 7.64; found: C 72.04, H 7.81%. FABMS (m/z) 550 M^+.

2.3.3. (*S*)-(+)-2-Methylbutyl 4-(6-acryloyloxy-hexyloxycinnamoyloxy) benzoate (***M4***)

Yield: 49.8%. K 57.3 °C S_A^* 67.8 °C I. $[\alpha]_D = +1.4°$. FTIR (KBr pellet, ν_{max}/cm^{-1}): 2933, 2875 (CH_2), 1705 (C=O in Ar–COO–), 1608, 1510 (C–C in Ar), 1195, 1226 (COC), 1675 (C=C), 982 (*E* form C=C). ^{1}H NMR ($CDCl_3$, δ in ppm): 0.91–1.02 (m, 6H, CH_3), 1.31–1.87 (m, 11H, CH_2), 3.99–4.03 (t, 2H, CH_2OPh, J = 6.34 Hz), 4.12–4.34 (t, 4H, $COOCH_2$, J = 6.61 Hz), 5.80–5.84 (dd, 1H, CH_2=CH, J = 10.34 Hz), 6.12 (dd, 1H, CH_2=CH, J_1 = 10.31 Hz, J_2 = 7.05 Hz), 6.37–6.43 (dd,

1H, CH=CH, $J = 17.12$ Hz), 6.45–6.51 (dd, 1H, CH=CH, $J = 15.88$ Hz), 6.91–6.93 (d, 2H, Ar–H, $J = 8.58$ Hz), 7.23–7.26 (d, 2H, Ar–H, $J = 8.51$ Hz), 7.52–7.55 (d, 2H, Ar–H, $J = 8.53$ Hz), 7.81–7.86 (dd, 1H, CH=CH, $J = 15.91$ Hz), 8.08–8.11 (d, 2H, Ar–H, $J = 8.47$ Hz). ^{13}C NMR (100.6 MHz, $CDCl_3$): 16.47 (CH_3), 25.65, 28.13, 28.37, 28.96 (CH_2), 34.25 ($CHCH_3$), 64.41, 65.15, 67.92 (OCH_2), 114.89, 121.59, 130.09, 131.03 (aromatic), 128.51, 130.49 (C=C), 113.92, 146.91 (C=C in cinnamoyl); 126.53, 127.83, 154.49, 161.39 (aromatic quaternary), 165.12, 165.91, 166.24 (C=O). From the UV–vis spectrum, $\lambda_{max} = 320$ nm ($CHCl_3$). Anal calcd for $C_{30}H_{36}O_7$: C 70.87, H 7.09; found: C 70.68, H 7.04%. FABMS (m/z) 508 M^+.

2.3.4. Ethyl 4-[4-(6-acryloyloxyhexyloxy)phenylazo] benzoate (*M5*)

Yield: 60.8%. K 72.8 °C N 87.5 °C I. FTIR (KBr pellet, ν_{max}/cm^{-1}): 2942, 2860 (CH_2), 1680 (C=C). ^{1}H NMR ($CDCl_3$, δ in ppm): 1.24–1.28 (t, 3H, CH_3), 1.30–1.85 (m, 8H, CH_2), 4.03–4.06 (t, 2H, CH_2OPh, $J = 6.55$ Hz), 4.13–4.16 (t, 2H, OCH_2, $J = 6.74$ Hz), 4.38–4.43 (t, 2H, OCH_2, $J = 7.13$ Hz), 5.80–5.83 (dd, 1H, CH_2=CH, $J = 9.10$ Hz), 6.08–6.15 (dd, 1H, CH_2=CH, $J_1 = 17.39$ Hz, $J_2 = 10.39$ Hz), 6.37–6.42 (dd, 1H, CH_2=CH, $J = 17.31$ Hz), 7.00–7.03 (d, 2H, Ar–H, $J = 8.46$ Hz), 7.88–7.96 (d, 4H, Ar–H, $J = 8.52$ Hz), 8.16–8.19 (d, 2H, Ar–H, $J = 8.38$ Hz). ^{13}C NMR (100.6 MHz, $CDCl_3$): 14.48 (CH_3), 24.82, 25.70, 28.78, 29.22 (CH_2), 61.81, 62.99, 68.17 (OCH_2), 110.46, 123.41, 127.72, 130.43 (aromatic), 128.81, 131.85 (C=C), 134.07, 146.46, 154.40, 166.65 (aromatic quaternary), 165.53, 166.31 (C=O). From the UV–vis spectrum, $\lambda_{max} = 360$ nm ($CHCl_3$). Anal calcd for $C_{24}H_{28}N_2O_5$: C 67.92, H 6.60, N 6.60; found: C 68.05, H 6.52, N 6.64%. FABMS (m/z) 424 M^+.

2.4. Synthesis of homopolymer (*P1*) and copolymers (*CP1–CP6*) (Scheme 3)

Homopolymer and copolymers were obtained by the polymerization of monomers in benzene in the presence of 3 mol% of 2,2′-azobisisobutyronitrile (AIBN) at 60 °C for 24 h. The feed molar ratio of 80/20 and 68/17/15 of the comonomers was used to prepare binary copolymers and ternary copolymers, respectively. The general synthetic procedures for the polymers are as follows: to a solution of a predetermined amount of monomers in benzene with 3 mol% of 2,2′-azobisisobutyronitrile (AIBN), the monomers were poured into a glass polymerization tube equipped with a sealing cap, which was degassed in vacuum by using a freeze–thaw technique, and then sealed. After completion of polymerization, the polymers were precipitated in a large amount of methanol solution, and the crude polymers were purified by dissolving them in benzene. This was followed by re-precipitation into methanol, and drying in vacuum. The chemical structures of homopolymer **P1** and copolymers **CP1–CP6** are shown in Scheme 3.

P1: **M1** (0.2 g, 0.427 mmol), AIBN (2.1 mg, 0.0128 mmol), and benzene (2 mL) were used. Yield: 65.8%. FTIR (KBr pellet, ν_{max}/cm^{-1}): 2943, 2863 (CH_2), 1730 (C=O in Ar–COO–), 1607, 1509 (C–C in Ar), 1257, 1198 (COC). ^{1}H NMR ($CDCl_3$ δ in ppm): 0.89 (m, 3H, CH_3), 1.25–1.74 (m, 19H, CH_2), 3.91–4.04 (m, 6H, CH_2O), 6.84–6.94 (m, 4H, Ar–H), 7.02–7.08 (m, 2H, Ar–H), 8.04 (m, 2H, Ar–H). Anal calcd for feed: C 71.79, H 7.69; found: C 71.42, H 7.35%.

CP1: **M1** (159.05 mg, 0.340 mmol), **M2** (40.95 mg, 0.085 mmol), AIBN (2.09 mg, 0.0127 mmol), and benzene (2 mL) were used. Yield: 65.7%. FTIR (KBr pellet, ν_{max}/cm^{-1}): 2940, 2862 (CH_2), 1728 (C=O in Ar–COO–), 1607, 1508 (C–C in Ar), 1255, 1199 (COC). ^{1}H NMR ($CDCl_3$, δ in ppm): 0.90–0.99 (m, CH_3), 1.25–1.76 (m, CH_2), 3.93 (m, OCH_2), 6.88 (m, Ar–H), 7.04 (m, Ar–H), 7.26 (m, Ar–H), 8.07 (m, Ar–H). Anal calcd for feed: C 71.37, H 7.90; found: C 71.33, H 7.55%.

CP2 was prepared by a procedure similar to that for **CP1**, using **M3** instead of **M2**. Yield: 70.5%. FTIR (KBr pellet, ν_{max}/cm^{-1}): 2941, 2868 (CH_2), 1727 (C=O in Ar–COO–), 1609, 1509 (C–C in Ar), 1246, 1199 (COC). ^{1}H NMR ($CDCl_3$, δ in ppm): 0.78–0.90 (m, CH_3), 1.01–1.93 (m, CH_2), 3.93–3.97 (m, CH_2O), 4.92 (m, $OCHCH_2$), 6.89 (m, Ar–H), 7.04 (m, Ar–H), 7.26 (m, Ar–H), 8.08 (m, Ar–H). Anal calcd for feed: C 71.84, H 7.68; found: C 71.85, H 7.67%.

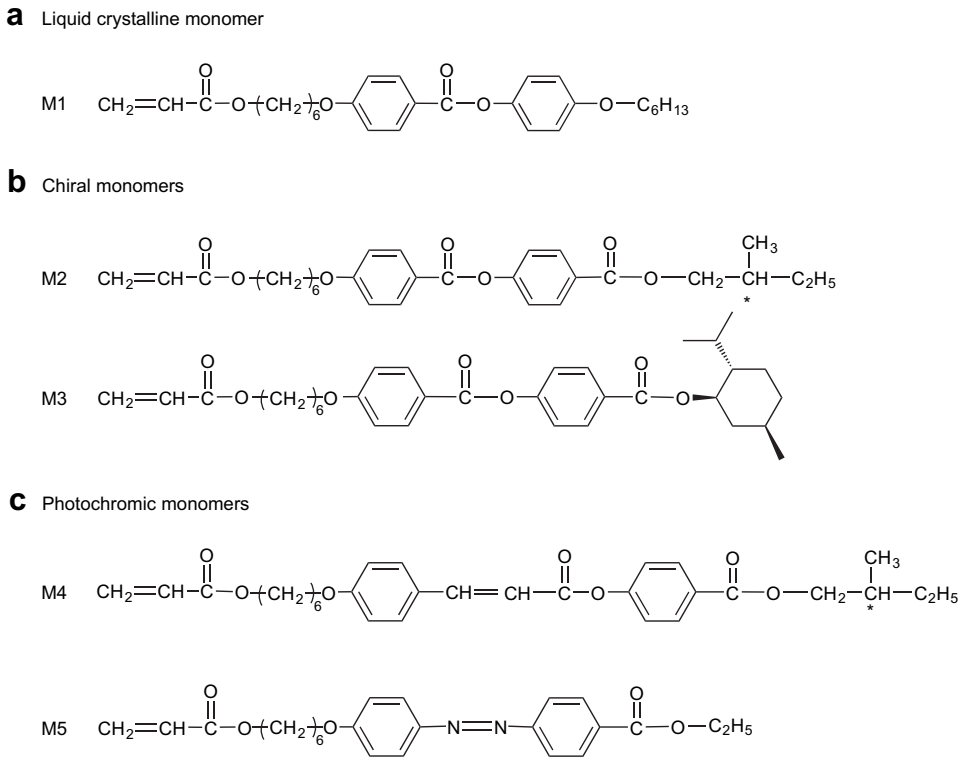

Scheme 1. Chemical structures of monomers with various functional groups.

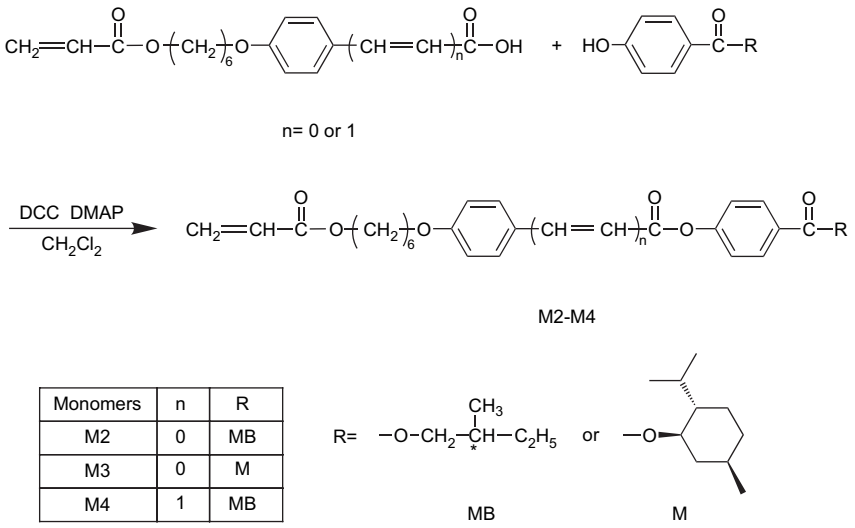

Monomers	n	R
M2	0	MB
M3	0	M
M4	1	MB

Scheme 2. Synthetic routes of monomers **M2**–**M4**.

CP3 was prepared by a procedure similar to that for **CP1**, using **M4** instead of **M2**. Yield: 60.9%. FTIR (KBr pellet, ν_{max}/cm^{-1}): 2937, 2870 (CH_2), 1715 (C=O in Ar–COO–), 1612, 1508 (C–C in Ar), 1230, 1202 (COC), 956 (*E* form C=C). ^1H NMR ($CDCl_3$, δ in ppm): 0.76–0.92 (m, CH_3), 1.07–2.05 (m, CH_2), 3.96–4.15 (m, CH_2O), 6.51–8.08 (m, Ar–H and vinyl H in cinnamoyl group). Anal calcd for feed: C 71.60, H 7.56; found: C 71.52, H 7.52%.

CP4: **M1** (137.33 mg, 0.293 mmol), **M2** (35.34 mg, 0.073 mmol), **M5** (27.42 mg, 0.065 mmol), AIBN (2.12 mg, 0.0129 mmol), and benzene (2 mL) were used. Yield: 58.2%. FTIR (KBr pellet, ν_{max}/cm^{-1}): 2940, 2859 (CH_2), 1725 (C=O in Ar–COO–), 1606, 1504 (C–C in Ar), 1257, 1189 (COC), 956 (*E* form C=C). ^1H NMR ($CDCl_3$, δ in ppm): 0.90–0.99 (m, CH_3), 1.33–2.29 (m, CH_2), 3.93–4.36 (m, OCH_2), 6.88 (m, Ar–H), 7.04 (m, Ar–H), 7.62 (m, Ar–H), 7.89 (m, Ar–H), 8.07 (m, Ar–H). Anal calcd for feed: C 70.90, H 7.43, N 0.91; found: C 71.06, H 7.48, N 1.00%.

CP5 was prepared by a procedure similar to that for **CP4**, using **M3** instead of **M2**. Yield: 47.5%. FTIR (KBr pellet, ν_{max}/cm^{-1}): 2942, 2862 (CH_2), 1726 (C=O in Ar–COO–), 1607, 1502 (C–C in Ar), 1255, 1194 (COC), 958 (*E* form C=C). ^1H NMR ($CDCl_3$, δ in ppm): 0.79–0.90 (m, CH_3), 1.11–2.30 (m, CH_2), 3.93 (m, OCH_2), 4.38 (m, $COOCH_2$), 4.92 (m, COOCH), 6.88 (m, Ar–H), 7.04 (m, Ar–H), 7.88 (m, Ar–H), 8.07 (m, Ar–H). Anal calcd for feed, C 71.32, H 7.54, N 0.88; found: C 70.76, H 7.57, N 0.91%.

CP6 was prepared by a procedure similar to that for **CP4**, using **M4** instead of **M2**. Yield: 60.1%. FTIR (KBr pellet, ν_{max}/cm^{-1}): 2945, 2863 (CH_2), 1728 (C=O in Ar–COO–), 1608, 1507 (C–C in Ar), 1259, 1203 (COC), 956 (*E* form C=C). ^1H NMR ($CDCl_3$, δ in ppm): 0.90 (m, CH_3), 1.33–2.27 (m, CH_2), 3.93–4.39 (m, OCH_2), 6.88 (m, Ar–H), 7.05 (m, Ar–H), 7.88 (m, Ar–H), 8.07 (m, Ar–H). Anal calcd for feed: C 71.10, H 7.43, N 0.90; found: C 71.07, H 7.44, N 0.99%.

2.5. Fabrication of liquid crystalline polymer films

Glass plates were cleaned using a detergent solution, and washed with water and acetone using ultrasonic equipment for 20 and 60 min, respectively. After completion of the cleaning process, the plates were dried in a vacuum. One of the glass surfaces was coated with polyvinyl alcohol ($M_w = 20{,}000$), dried and then rubbed. A glass cell with a pair of parallel pre-rubber plates and a 25 μm gap was fabricated. The polymer was heated to the isotropic phase and then coated on a glass surface, cooled to the liquid

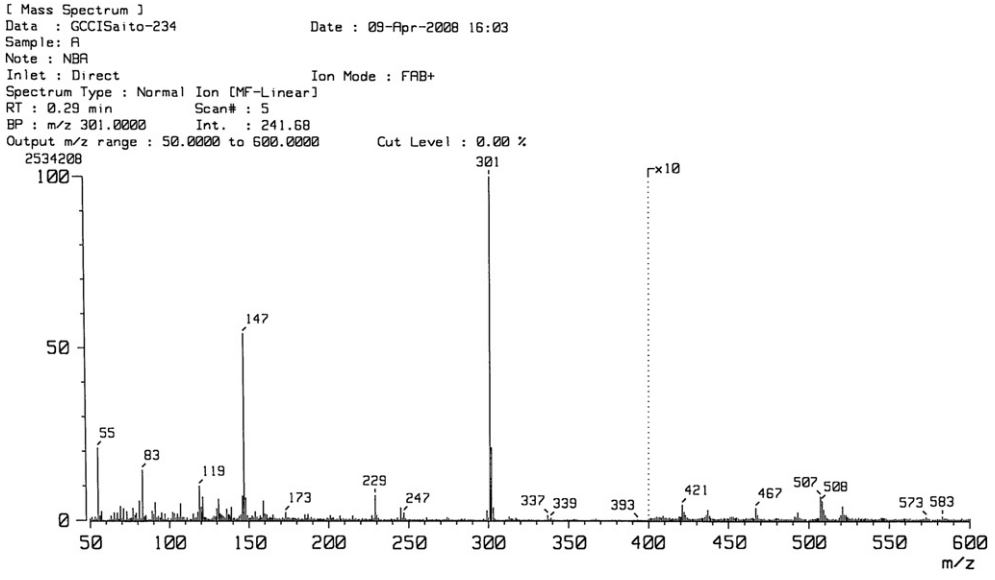

Fig. 1. FABMS (Fast Atom Bombardment Mass Spectroscopy) spectrum of monomer **M4**.

crystal phase and then sandwiched with another glass plate. The cholesteric polymer film was achieved by thermal annealing under the liquid crystal phase temperature for 40–60 min. The optical properties of the liquid crystalline polymer films were investigated.

3. Results and discussion

3.1. Synthesis and characterization

In order to investigate the photoreactivity of liquid crystalline copolymers with multiple photochromic groups, a series of side chain liquid crystalline polyacrylates incorporating liquid crystalline, chiral, and photochromic pendant groups were synthesized. Scheme 1 illustrates the chemical structures of the monomers with various functionalities. Typical synthetic routes for the target monomers **M2**–**M4** are shown in Scheme 2. Monomers synthesized in this investigation were identified using FTIR, EA, and NMR. Fig. 1 shows a FABMS (Fast Atom Bombardment Mass Spectroscopy) mass spectrum of monomer **M4**. Fig. 2 shows the ^{1}H and ^{13}C NMR spectra of chiral photochromic monomer **M4** in $CHCl_3$. Peaks for the carbons and protons were assigned with the letters of the numbers and alphabet as shown in the figure. ^{13}C NMR and DEPT-135 measurements were adapted to confirm the structure of **M4**, and the spectra agree well with the proposed molecular structure of **M4**. The ^{1}H NMR spectrum of **M4** showed peaks at 6.91–8.11, 5.80–6.43, and 0.91–0.96 ppm, corresponding to aromatic, vinyl, and methyl protons, respectively. In addition, the vinyl C=C protons of the cinnamoyl group appeared at 6.45–6.51 and 7.81–7.86 ppm. ^{13}C NMR and DEPT-135 measurements were adapted to confirm the structure of **M4**. In the aromatic region, four resonance peaks at 126.53, 127.83, 154.49, and 161.39 ppm are peculiar to quaternary carbons (C_9, C_{10}, C_{16}, and C_{17}), which are consistent with the disappearance of peaks in DEPT-135. Furthermore, signals arising from CH_2 groups (C_4, C_8, C_{21}, etc.) exhibited negative peaks. The aromatic protons at position H_l appeared at the most downfield (8.10 ppm) as a doublet.

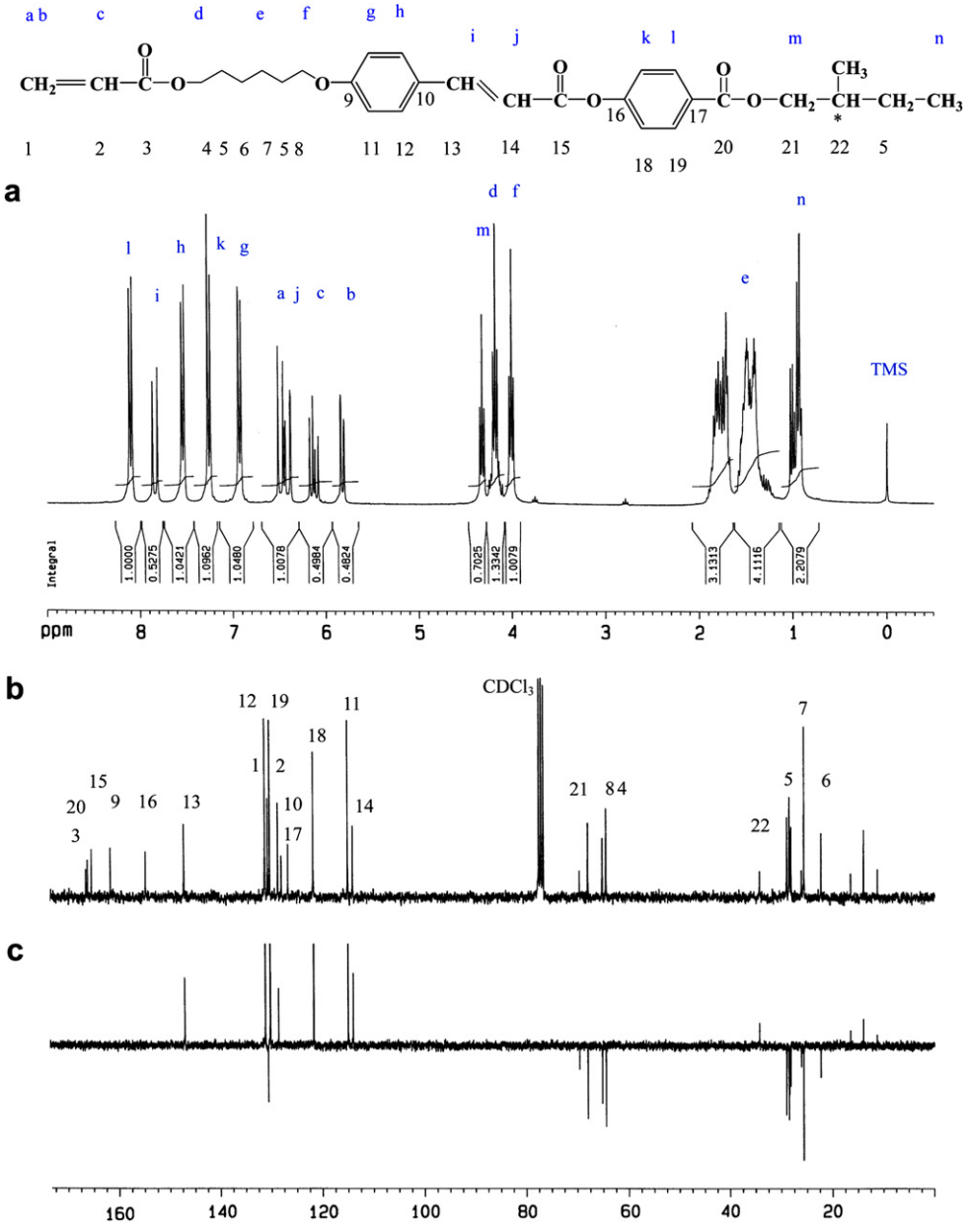

Fig. 2. (a) ^{1}H, (b) ^{13}C NMR and (c) DEPT-135 spectra of chiral monomer **M4**.

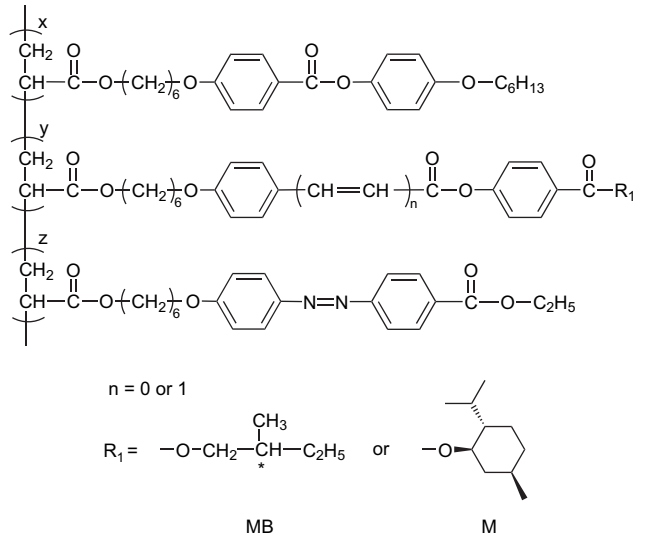

Scheme 3. Chemical structures of homopolymer and copolymers.

Table 1
Phase transition temperature (°C), enthalpy changes[a] (J/g) and specific rotation of monomers

Monomer	Phase transition (°C); enthalpy changes (J/g)		$[\alpha]_D$[c] (°)
	Heating cycle[b]	Cooling cycle[b]	
M1	K 57.0 N 62.0 I; 30.4, 2.3	I 36.9 K; −16.4	–
M2	K 16.8 S_A^* 24.0 I; 18.7, 0.6	I 4.6 K; −14.5	+3.2
M3	K 32.6 I; 25.4	I 12.5 K; −7.9	−46.2
M4	K 57.3 S_A^* 67.8 I; 88.9, 6.9	I 64.5 S_A^* 17.1 K; −5.9, −24.4	+1.4
M5	K 72.8 N 87.5 I; 72.5, 12.4	I 84.6 N 39.6 K; −13.8, −58.0	–

[a] Enthalpy of the phase change during heating and cooling at a rate of 10 K min^{-1}.
[b] K, crystal; N, nematic; S_A^*, chiral smectic A; I, isotropic phase.
[c] Specific rotation of compounds, 0.1 g in 10 mL $CHCl_3$.

Homopolymerization and copolymerization of the synthesized monomers were carried out, and the polymer structures are shown in Scheme 3. The molecular weight, thermal decomposition temperature, and specific rotation of the polymers are summarized in Table 2. After polymerization, the corresponding signals of the vinyl group at 5.80–6.43 ppm in the ^{1}H NMR spectra disappeared completely. The peaks of the chemical shifts corresponding to the polymer were quite broad and consistent with the expected polymer structure. The weight-average molecular weights (M_ws) of **P1** and **CP1**–**CP6** were 3.3×10^4 and $1.2–1.6 \times 10^4$ g mol^{-1}, respectively. The polydispersity index (PDI) was between 1.49 and 2.01. Flexible hexyloxy (–OC_6H_{13}) side groups solubilized the synthesized polymers readily, in common organic solvents such as chloroform, toluene, and THF. The thermal stability of the synthesized polymers under nitrogen atmosphere was evaluated by TGA, which indicated that the degradation temperature of 5% weight

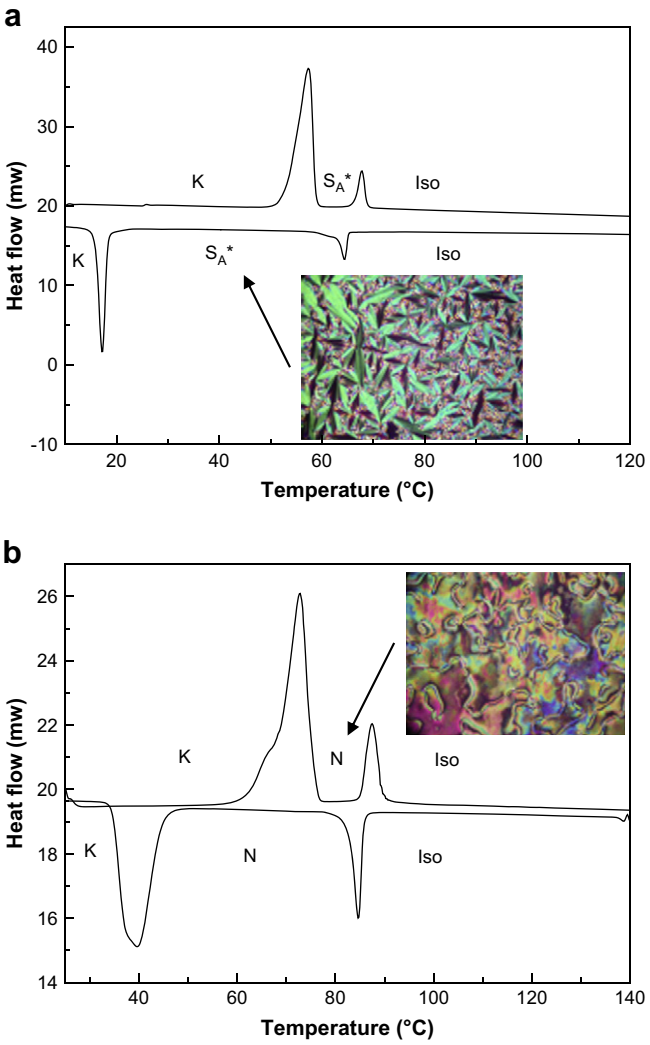

Fig. 3. DSC thermograms of compounds (a) **M4** and (b) **M5**. Insets (a) and (b): polarizing microscopic textures of **M4** and **M5** at the corresponding state indicated in the figures (100× magnification).

Table 2
Results of polymerization[a]

Polymer	Phase transition temperature[b] (°C)		Composition		M_w[d] ($\times 10^4$)	PDI[d]	T_d[e] (°C)	$[\alpha]_D$[f] (°)
	Heating cycle	Cooling cycle	Comonomer	$x/y/z$[c]				
P1	G 18.2 S_A 115.0 I	I 108.8 S_A 20.5 G	**M1**	–	3.3	1.89	404.7	–
CP1	G 16.5 N* 100.1 I	I 98.5 N* 14.5 G	**M1**/**M2**	78.2/21.8/0	1.5	1.69	396.3	+1.1
CP2	G 26.3 N* 92.2 I	I 94.8 N* 22.3 G	**M1**/**M3**	75.4/24.6/0	1.4	1.71	373.0	−9.2
CP3	G 16.5 N* 125.0 I	I 116.2 N* 13.8 G	**M1**/**M4**	72.5/27.5/0	1.6	1.52	395.6	+0.8
CP4	G 17.7 N* 105.6 I	I 102.3 N* 12.8 G	**M1**/**M2**/**M5**	76.5/7.0/16.5	1.2	1.62	397.2	+0.7
CP5	G 22.0 N* 88.2 I	I 88.5 N* 19.0 G	**M1**/**M3**/**M5**	68.9/18.5/12.6	1.4	2.01	375.8	−8.2
CP6	G 22.5 N* 92.0 I	I 97.0 N* 25.5 G	**M1**/**M4**/**M5**	69.4/14.1/16.5	1.3	1.49	390.5	+0.6

[a] In benzene at 60 °C for 24 h in the presence of 3 mol% AIBN.
[b] G, glassy; S_A, smectic A; N*, chiral nematic; I, isotropic phase.
[c] Feed molar ratio $x/y/z = 80/20/0$ for binary system **CP1**–**CP3** and $x/y/z = 68/17/15$ for ternary system **CP4**–**CP6**; final molar ratio was estimated by ^{1}H NMR spectroscopy.
[d] M_w, and PDI of the polymers were determined by gel permeation chromatography using polystyrene standards in $CHCl_3$.
[e] The initial decomposition temperature at 5% weight loss; measured by TGA at a heating rate of 40 K min^{-1}.
[f] Specific rotation of compounds, 0.1 g in 10 mL $CHCl_3$.

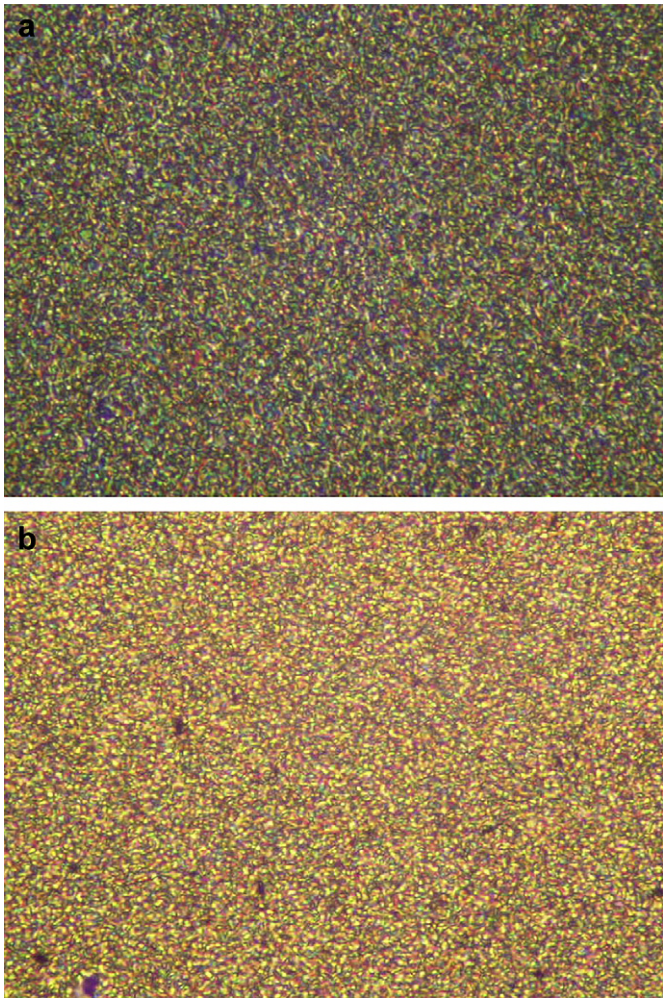

Fig. 4. Polarizing micrographs of the liquid crystalline texture of the polymers: (a) **CP4** at 62.5 °C while cooling from the isotropic state and (b) **CP5** at 56.4 °C while heating from the glass transition (400× magnification).

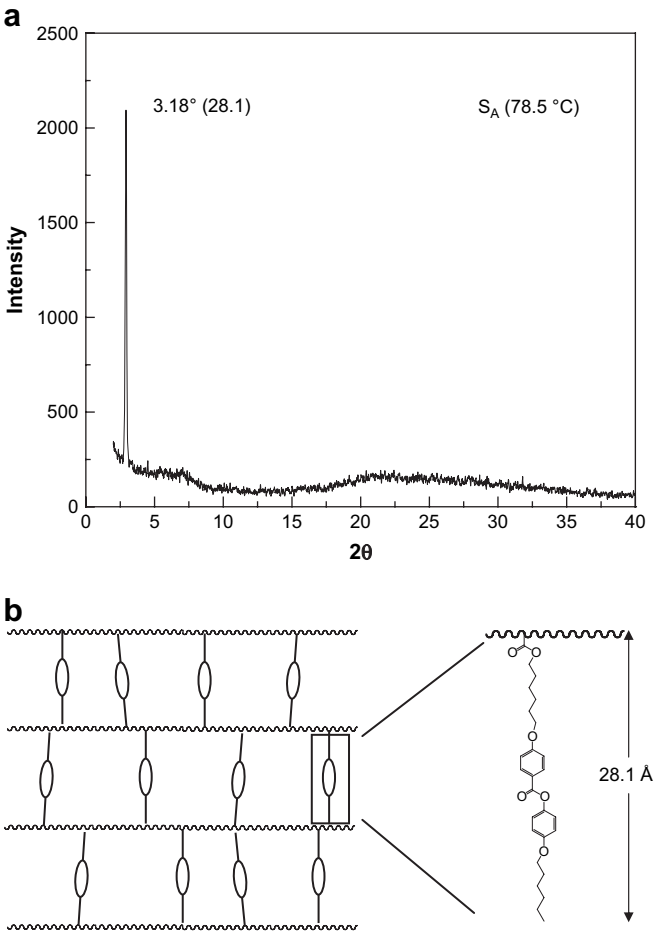

Fig. 5. (a) X-ray diffraction pattern of polymer **P1** and (b) schematic representation for the smectic monolayer arrangement in **P1**.

loss (T_d) in nitrogen was greater than 373 °C, and about 50% weight loss occurred beyond 440 °C for all polymers, indicating that the synthesized polymers have a higher thermal stability. The results suggest that the existence of the longer mesogenic side chain might cause a strong interaction between the repeating units leading to the increase of thermal stability.

3.2. Thermal and liquid crystalline properties

The corresponding phase transition temperatures and the phases of the synthesized monomers and polymers, obtained during the first cooling and the second heating cycles, are summarized in Tables 1 and 2. The phase of liquid crystalline textures was confirmed by DSC and X-ray diffraction analyses, and was also compared with polarized optical microscopic (POM) textures reported in the literature [30]. The data listed in Table 1 revealed that the effect of molecular structures on phase transition temperatures of monomers was considerable. The results suggest that the rigidity of the mesogenic core, the flexible spacer length, and terminal units highly influence the melting temperature, mesophase temperature, and even molecular arrangement. In other words, polarity and spacer length at the center and terminals play an important role in the formation of liquid crystalline phases. **M4** showed a melting transition at 57.3 °C and a chiral smectic-to-isotropic phase transition at 67.8 °C on the heating scan. During the cooling scan, an isotropic-to-chiral smectic phase transition at 64.5 °C and crystallization at 17.1 °C were observed. The DSC curves and POM textures of monomers **M4** and **M5** at a heating rate of 10 K min^{-1} are summarized in Fig. 3. As shown in Fig. 3, the chiral smectic (S_A^*; fan-shape texture) and nematic (N; schlieren texture) characteristics for **M4** and **M5** were examined, respectively.

As shown in Scheme 3, the polymers were all rod-like molecules, and contain high polar hindered pendant groups. Also, as

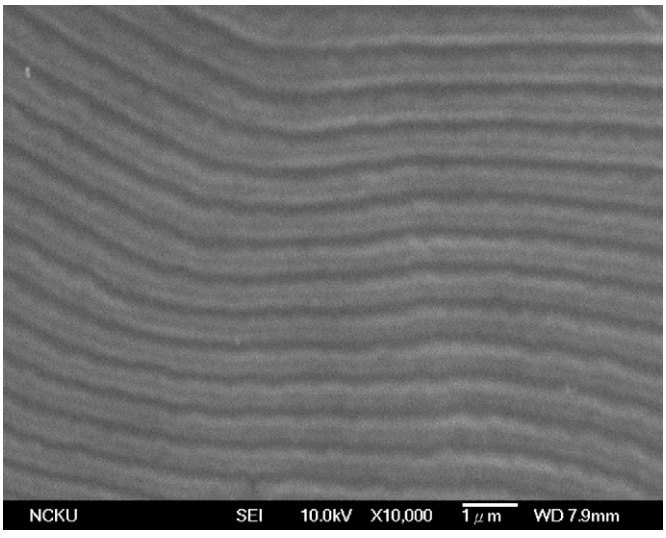

Fig. 6. Side view of SEM photograph of cholesteric polymer film **CP2**.

Table 3
Optical properties of photochromic monomers

Monomer	λ_{max}[a] (nm)	ε at λ_{max}[b]	Isosbestic[c]	t_{300}[d] (s)	t_{dark}[d] (min)
M4	320	2.46×10^4	268, 351	2.1×10^3	–
M5	360	2.51×10^4	313, 420	20[e]	9.0×10^2

[a] Maximum wavelength of the π–π^* transition of the photochromic monomers in chloroform solution.
[b] Absorption coefficients (M^{-1} cm^{-1}) of monomers at λ_{max} of the corresponding monomers.
[c] Isosbestic points (nm) in absorption during UV irradiation.
[d] t_{300}: time reached the photostationary state of UV irradiation ($\lambda_{irr} = 300$ nm) t_{dark}: time reached the photostationary state in the dark.
[e] Time reached the photostationary state of UV irradiation ($\lambda_{irr} = 365$ nm).

Table 4
UV–vis absorption of photochromic copolymers

Sample	λ_{max}[a] (nm)	t_{365}[b] (s)	Sample	λ_{max}[a] (nm)	t_{365}[b] (s)
P1	268	–	**CP4**	265, 360	30
CP1	266	–	**CP5**	264, 358	25
CP2	266	–	**CP6**	264, 356	1.8×10^2[c], 25
CP3	242, 320	1.2×10^3[c]			

[a] Maximum wavelength of the π–π^* transition of the photochromic copolymers; concentration: 1×10^{-5} M in chloroform solution.
[b] Time reached the photostationary state of UV irradiation (365 nm).
[c] Time reached the photostationary state of UV irradiation (300 nm).

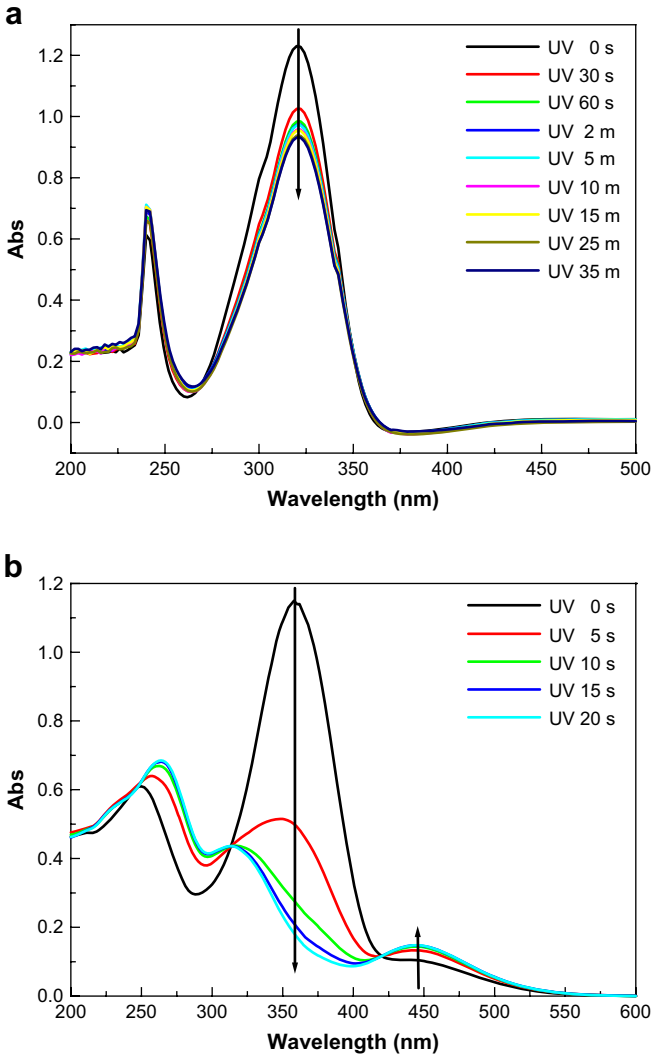

Fig. 7. UV–vis spectra before and after UV irradiation with 300 nm for (a) **M4** and with 365 nm for (b) **M5**.

shown in Table 2, all polymers were revealed to have high interaction between side chain units, leading to the formation of liquid crystalline phases. The difference in the mesogenic core and the terminal groups of these monomers might affect both monomer interaction and polymerization rate leading to the variation of yields, final molar ratio, and molecular weight of polymers. The specific rotation of chiral polymers having various groups was estimated. Theoretically, chirality plays an important role in cholesteric liquid crystals. The chirality of the chiral polymers can be expected to affect the arrangement and the helical pitch of chiral liquid crystals by adding them in liquid crystals as dopants. As shown in Scheme 3 and Table 2, achiral homopolymer **P1**, containing a terminal electron releasing hexyloxy ($-OC_6H_{13}$) group, exhibited a smectic A phase (S_A; fan-shaped texture). Regarding these results, all copolymers (**CP1**–**CP6**) containing chiral pendant groups possessed chiral nematic (N^*; oily streaks texture) phases due to the disturbances in molecular orientation by the sterically hindered fragment of the chiral units in copolymers, leading to a decrease in lateral molecular interactions and the appearance of chiral nematic phases. Fig. 4 shows the POM textures of **CP4** and **CP5**. Cleavage of the double bond and the binding of other monomers together did not seem to significantly affect the chirality of the compounds. The results also indicate that the specific rotation depends not only on the content of chiral units in polymers, but also on the differences in the chirality, molecular weight, and copolymer composition. It also suggests that the specific rotation was influenced by the coherence of polarity due to chemical bonding after polymerization. As compared to binary copolymers **CP1**–**CP3**, the results in Table 2 show a decrease in the molar content of chiral units in ternary copolymers **CP4**–**CP6**, which could also induce chiral nematic phases. Furthermore, the phase transition temperature and thermal stability of the ternary copolymers are similar to those of binary copolymers.

To further elucidate the structures of the liquid crystalline phases, representative X-ray diffraction measurements of homopolymers and copolymers were made. Samples were heated to the temperature range of the mesophases and then quenched. As shown in Fig. 5(a), the X-ray diffraction curve of homopolymer **P1** showed a sharp peak at $2\theta = 3.18°$, corresponding to the layer *d*-spacing value of 28.1 Å at 78.5 °C. Furthermore, a fan-shaped texture could be clearly observed by POM, which is a characteristic texture of the smectic A phase. According to the molecular modeling calculation using CS Chem3DPro, employing MM2 energy parameters, the estimated all-*trans* molecular length *l* of the most extended conformation of monomer **M1** is around 28.3 Å (the layer *d*-spacing value is ca. 28.1 Å by X-ray diffraction patterns; $l/d = 0.99$). Therefore, a possible layer structure of **P1** is suggested to exhibit monolayer packing of side chains. Fig. 5(b) illustrates the schematic representation for the smectic monolayer arrangement in **P1**. The X-ray diffraction patterns of copolymers **CP1**–**CP6** showed a typical nematic characteristic with a broad peak in the region of $2\theta = 15$–$30°$, classically due to the average lateral distance between the neighboring chains with *d*-spacing of 3–5 Å at the temperature ranges of the mesophases [31]. From the evidence of the layer structures of the polymers, homopolymer **P1** showed the molecular packing of the smectic phase. However, copolymers **CP1**–**CP6** exhibited the nematic characteristic due to the disrupting of molecular orientation by the chiral monomers with steric hindered fragment into the copolymers, leading to the absence of the smectic phases.

Copolymer **CP2** was coated on a substrate with 25 μm thickness. Fig. 6 shows a side view of the SEM image of the helical structure of **CP2** after thermal annealing under the temperature range of the mesophase and subsequent quenching. The pitch length (about 563 nm) of the cholesteric polymeric film of **CP2** was estimated. Theoretically, the pitch is influenced by the molecular chirality, the

content of the chiral unit, and the molecular interaction between molecules. The undulating texture in the helical structure might be due to the unsophisticated process of cutting and thermal annealing treatments.

3.3. Optical properties and E/Z photoisomerization

To study the photoreactivity of liquid crystalline copolymers with multiple photochromic groups, configurational *E*/*Z* isomerization of photochromic monomers **M4**/**M5** and copolymers **CP1**–**CP6** was studied. Tables 3 and 4 summarize the data on the absorption and absorption coefficient of the photochromic monomers and copolymers. Photoisomerism of all monomers and polymers was monitored by UV absorption spectra in a chloroform solution exposed with 300 and 365 nm UV light. **M4** containing a cinnamoyl group in the *E* form showed a strong absorbing band at 320 nm with $\varepsilon = 2.46 \times 10^4\ M^{-1}\ cm^{-1}$, attributed to the π–π^* electronic transition of the *E*-form isomers in the chloroform solution. Fig. 7(a) and (b) presents the UV–vis spectra before and after UV irradiation with 300 nm for **M4** and with 365 nm for **M5**, respectively. UV irradiation caused a decrease in the absorption band at around 320 nm with an increase during the UV ($\lambda_{irr} = 300$ nm) irradiation time period for **M4**. The decrease was induced by the *E*–*Z* photoisomerization at the C=C segment. On the contrary, azo monomer **M5** exhibited an absorption maximum at around 360 nm and a weak shoulder at around 445 nm related to π–π^* and n–π^* transitions of the *E*-form azobenzene, respectively. Isosbestic points at 268 and 351 nm for monomer **M4** were observed during the procedure of UV irradiation which corresponds to *E*–*Z* photoisomerization [32]. As compared to **M4**, azo monomer **M5** with an N=N segment revealed isosbestic points at 313 and 420 nm as shown in Fig. 7(b). A steady state for *E*–*Z* transition was completely achieved in 35 min for **M4**. Nevertheless, as seen in Fig. 7(b), the steady state for *E*–*Z* transition was completely achieved in only 20 s for azo monomer **M5**, due to the lower energy band gap of azobenzene derivatives as compared to that of cinnamoyl-containing monomers with C=C segments. Azobenzene derivatives are characterized by reversible transformations from the generally more stable *E* form to the unstable *Z* form upon irradiation with UV or visible light to yield a photostationary composition that is both temperature and wavelength dependent [33]. UV irradiation caused a decrease of about 360 nm and an increase at about 445 nm for **M5**. As shown in Fig. 7(b), the π–π^* band shifted to a shorter wavelength, and the intensity of the n–π^* absorption increased. The variation of the absorptions might have been due to the geometric change from *E* to *Z* of the azo monomer during UV irradiation. The absorption stability of the monomers in dark surroundings was also studied. The thermal stability of **M5** was around 15 h. The results indicate that the geometric *Z* form might return to the *E* form gradually, even without any exposure to UV light.

To understand the specific photo-optical behaviors of binary or ternary copolymers with one or dual photochromic groups, it is essential to understand the photochemical processes that occur in chloroform solutions. Fig. 8(a) and (b) depicts the dependence of UV absorption of binary copolymer **CP3** and ternary copolymers **CP4**/**CP5** with one photochromic (C=C or N=N) segment with UV irradiation at 300 and 365 nm, respectively. Photoinduced

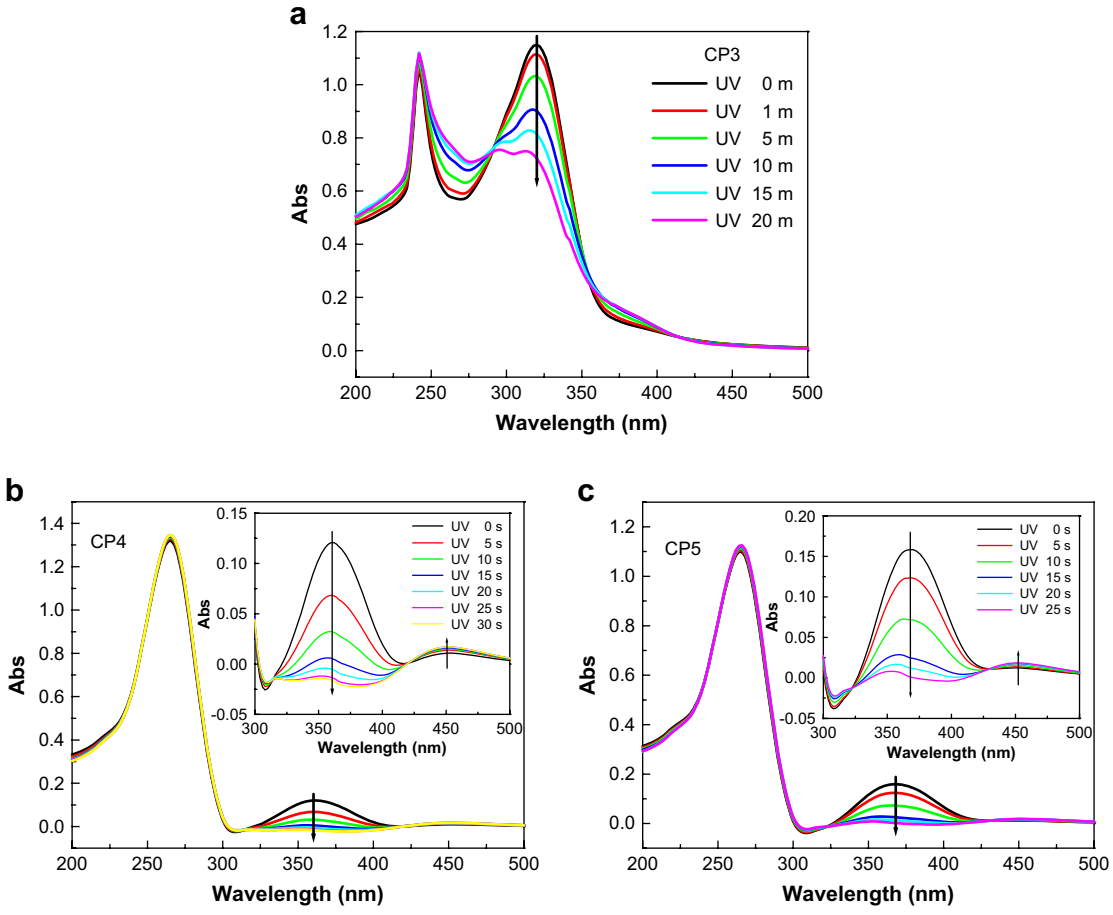

Fig. 8. UV–vis spectra for copolymers during UV irradiation with 300 nm for (a) **CP3** and with 365 nm for (b) **CP4**, and (c) **CP5**. Insets (b) and (c): UV absorption spectra of **CP4** and **CP5** at the corresponding state indicated in the figures.

configurational *E*/*Z* isomerization further changed the π-electron conjugation systems leading to a decrease at 320 nm for binary copolymer **CP3**. Contrary to binary photochromic copolymer **CP3** with a C═C bond, ternary copolymers **CP4** and **CP5** containing an N═N bond show two principal peaks: a longer wavelength peak (λ_{max} ~ 360 nm) which corresponds to the π–π* electron transition of the azobenzene groups, and a shorter wavelength peak (λ_{max} ~ 265 nm) corresponding to the π–π* electron transition of the mesogenic phenylbenzoate units (the longer wavelength peak at about 420–460 nm associated with the n–π* electron transition of the azobenzene groups was nearly unobservable due to a low extinction coefficient). The UV irradiation leads to significant changes in the absorption spectra of the copolymers. In this case, one might observe a marked decrease in the absorption peak associated with the π–π* electron transition of the azobenzene groups, whereas at λ_{max} ~ 265 nm, no remarkable changes in the absorption could be observed due to the absence of photochromic moieties for mesogenic phenylbenzoate units.

As shown in Fig. 9(a), for ternary copolymer **CP6** possessing dual photochromic (C═C and N═N) groups, a distinct decrease in the absorption peak associated with the π–π* electron transition of the azobenzene groups upon UV irradiation with 365 nm could be observed, whereas at λ_{max} ~ 264 nm, no remarkable changes in the absorption were observed. Such spectral changes suggested the occurrence of the *E*–*Z* photoisomerization relative to the N═N bond. In the case of the copolymer, spectral changes were less pronounced to the C═C bond. In other words, the cinnamoyl (C═C) group was not sensitive to 365 nm UV light and experienced almost no *E*–*Z* isomerization. Isomerization was observed only for azobenzene groups. However, as observed in Fig. 9(b), UV irradiation at λ_{irr} = 300 nm primarily led to changes in the shorter wavelength peak responsible for the C═C bond of the cinnamoyl groups. It also indicated that partial azobenzene groups underwent *E*–*Z* photoisomerization. Fig. 10 shows the variation in UV sensitivity for chloroform solution at room temperature for copolymer **CP6** during UV irradiation using two different wavelengths. Fig. 10(a) and (b) shows the variation in UV sensitivity of **CP6** with UV irradiation at 365 and 300 nm, respectively. Taking into account the above speculation, one might conclude that isomerization of various photochromic groups could be controlled by altering the wavelength of the irradiated light. It might indicate that the cinnamoyl photochromic groups were irreversibly transformed to the *Z* form whereas in the case of azobenzene groups, the *E*–*Z* isomerization was completely reversible. Accordingly, while selecting the wavelength of irradiated light, one might cause an exclusive

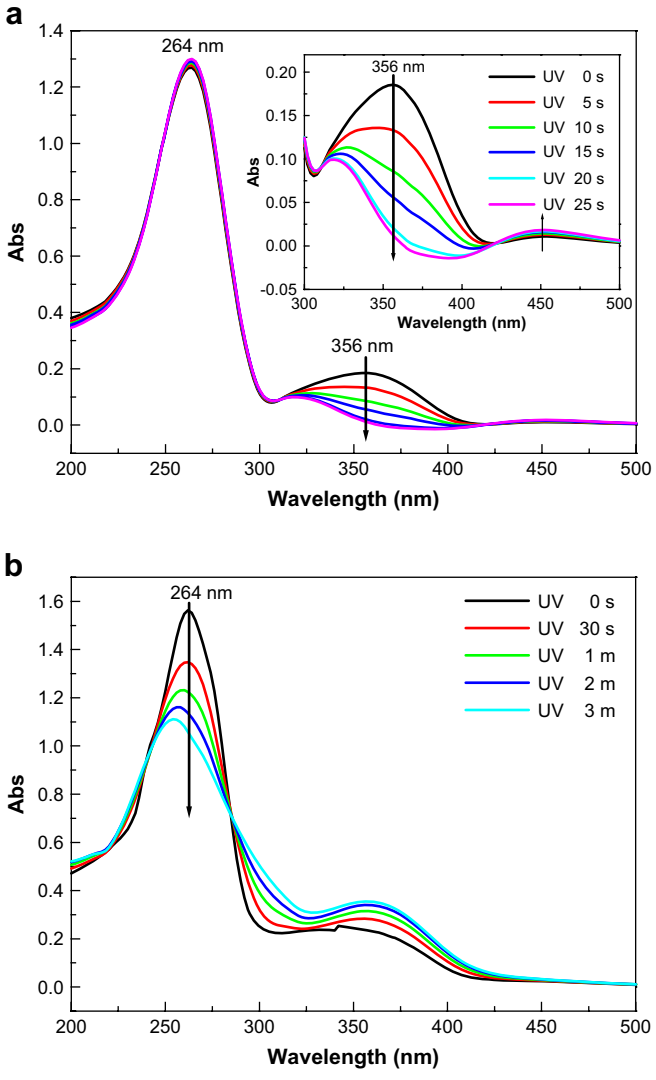

Fig. 9. Variation of the absorption spectra for chloroform solutions of copolymer **CP6** during UV irradiation with light of different wavelengths (a) 365 and (b) 300 nm. Inset (a): UV absorption spectra of **CP6** at the corresponding state indicated in the figure.

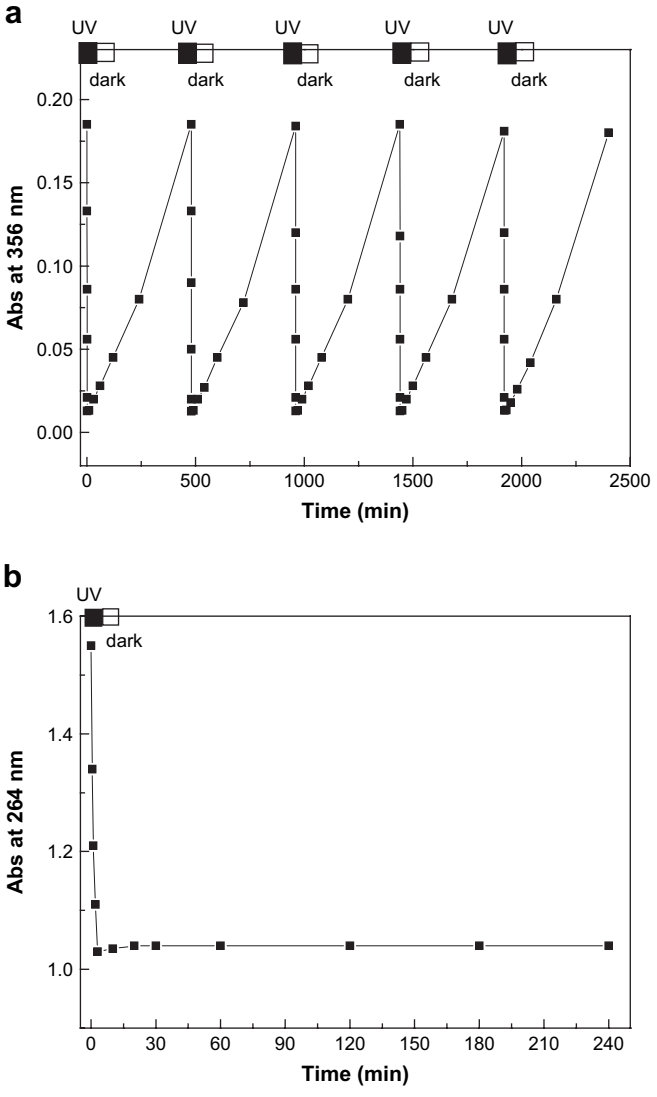

Fig. 10. Variation of UV sensitivity for chloroform solution at room temperature of copolymer **CP6** during UV irradiation and dark treatment with light of different wavelengths (a) 365 and (b) 300 nm.

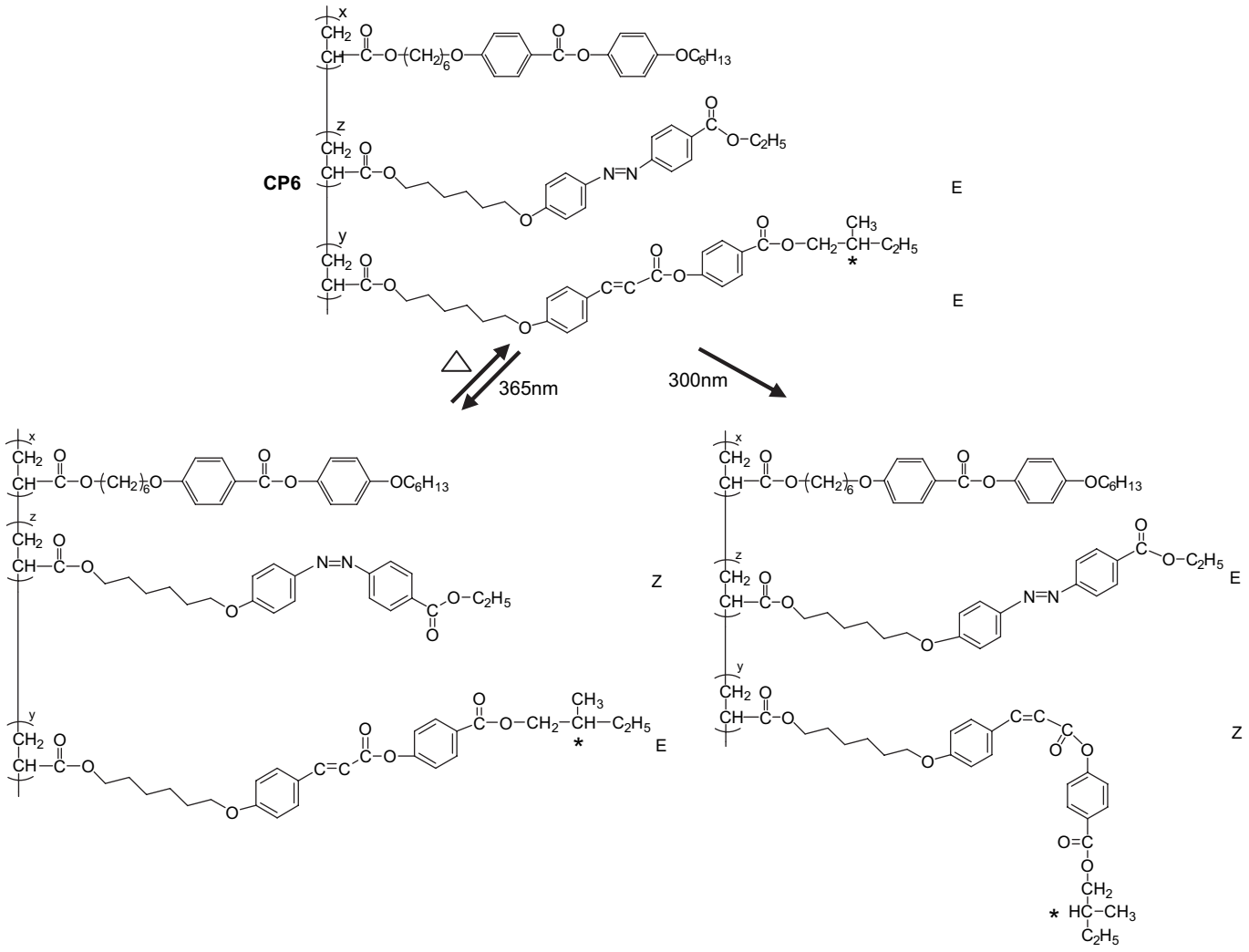

Scheme 4. Schematic representation of photoinduced mechanisms for copolymer **CP6** induced by the different irradiated wavelengths.

isomerization either of cinnamoyl (C═C) or azobenzene (N═N) photochromic groups as shown in Scheme 4. Such a copolymer presents a unique potential for controlling the properties of the polymer matrix due to reversible and irreversible photoisomerizations of azobenzene and cinnamoyl with respect to N═N and C═C bonds, respectively. Furthermore, the free volume, order parameter, and helical twisting power of polymers could be influenced as a consequence. The results of this investigation present significant scientific and practical contributions with respect to the development of unique multifunctional photochromic polymer materials.

4. Conclusions

A series of binary and ternary liquid crystalline copolymers with mono and dual photochromic segments were synthesized and characterized. As compared with binary copolymers, a decrease in the chiral unit content of the ternary copolymers did not significantly reduce the thermal stability and phase transition temperature. By selecting the wavelength of irradiated light, one might cause an exclusive isomerization of either cinnamoyl (C═C) or azobenzene (N═N) photochromic groups. Synthesized ternary liquid crystalline copolymers containing N═N and C═C photochromic segments revealed one reversible and one irreversible photochromic properties. From these results, the ternary multifunctional copolymers are expected to be of use in irreversible image recording and rewritable data storage systems.

Acknowledgements

The authors thank the National Science Council of the Republic of China (Taiwan) for financially supporting this research under Contract No. NSC 95-2221-E-006-190.

References

[1] Delaire JA, Nakatani K. Chem Rev 2000;100:1817.
[2] Meyer JG, Ruhmann R, Sumpe J. Macromolecules 2000;33:843.
[3] Zettsu N, Ubukata T, Seki T, Ichimura K. Adv Mater 2001;13:1693.
[4] Giménez R, Millaruelo M, Piñol M, Serrano JL, Viñuales A, Rosenhauer R, et al. Polymer 2005;46:9230.
[5] Uchida E, Kawatsuki N. Polymer 2006;47:2322.
[6] Cowie JMG, Hunter HW. J Polym Sci Part A Polym Chem 1993;31:1179.
[7] Zhang M, Schuster GB. J Am Chem Soc 1994;116:4852.
[8] Denekamp C, Feringa BL. Adv Mater 1998;10:1080.
[9] Bobrovsky AY, Boiko NI, Shibaev VP. Adv Mater 1999;11:1025.
[10] Hattori H, Uryu T. J Polym Sci Part A Polym Chem 2000;38:887.
[11] Bobrovsky A, Shibaev V. Polymer 2006;47:4310.
[12] Natansohn A, Rochon P, Pézolet M, Audet P, Brown D, To S. Macromolecules 1994;27:2580.
[13] Meng X, Natansohn A, Barrett C, Rochon P. Macromolecules 1996;29:946.
[14] Whitcombe MJ, Gilbert A, Mitchell GR. J Polym Sci Part A Polym Chem 1992;30:1681.
[15] Wu Y, Kanazawa A, Shiono T, Ikeda T, Zhang Q. Polymer 1999;40:4787.

[16] (a) Bobrovsky A, Boiko N, Shibaev V, Stumpe J. J Photochem Photobiol A 2004; 163:347;
(b) Tamaoki N, Song S, Moriyama M, Matsuda H. Adv Mater 2000;12:94.
[17] Giménez R, Piñol M, Serrano JL, Viñuales AI, Rosenhauer R, Stumpe J. Polymer 2006;47:5707.
[18] Liu JH, Wu FC, Lin TH, Fuh YG. Opt Express 2004;12:1857.
[19] Liu JH, Hsieh CD, Wang HY. J Polym Sci Part A Polym Chem 2004;42:1075.
[20] Liu JH, Yang PC, Lin TH, Chen YJ, Wu CH, Fuh YG. Appl Phys Lett 2005;86: 161120.
[21] Liu JH, Yang PC, Wang YK, Wang CC. Liq Cryst 2006;33:237.
[22] Liu JH, Yang PC. Polymer 2006;47:4925.
[23] Liu JH, Yang PC, Chiu YH, Suda Y. J Polym Sci Part A Polym Chem 2007;45: 2026.
[24] Liu JH, Yang PC. J Appl Polym Sci 2004;91:3693.
[25] Portugall M, Ringsdorf H, Zentel R. Makromol Chem 1982;183:2311.
[26] Bobrovsky AY, Boiko NI, Shibaev VP. Liq Cryst 1998;24:489.
[27] Ringsdorf H, Schmidt HW. Makromol Chem 1984;185:1327.
[28] Imric CT, Karasz FE, Attard GS. Macromolecules 1992;25:1278.
[29] Stewart D, Imric CT. Polymer 1996;37:3419.
[30] (a) Dierking I. Textures of liquid crystals. Weinheim: Wiley-VCH, ISBN 3-527-30725-7; 2003;
(b) Hans K, Rolf H. Handbook of liquid crystals. Weinheim: Verlag Chemie, ISBN 0895730081; 1980;
(c) , http://bly.colorado.edu/lcphysics/textures/.
[31] McArdle CB. Side chain liquid crystal polymers. NY, New York; 1989. ISBN: 0-216-92503-7.
[32] Sapich B, Stumpe J, Kricheldorf HR, Fritz A, Schönhals A. Macromolecules 2001;34:5694.
[33] Griffiths J. Photochemistry of azobenzene and its derivatives. Chem Soc Rev 1972;1:481.